ELSEVIER

Chemical Engineering Journal 139 (2008) 284–295

Chemical Engineering Journal

www.elsevier.com/locate/cej

Performance of Kenics static mixer over a wide range of Reynolds number

Vimal Kumar, Vaibhav Shirke, K.D.P. Nigam *

Department of Chemical Engineering, Indian Institute of Technology, Delhi, Hauz Khas, New Delhi 110016 India

Received 28 July 2007; accepted 31 July 2007

Abstract

The present study deals with the numerical simulation of flow patterns and mixing behaviour in Kenics static mixer over a wide range of Reynolds number. Three different sets of Kenics mixer (aspect ratio = 1.5) comprised of 3, 9 and 25 elements each have been characterized. The Reynolds number was varied in the range of 1 to 25,000 (i.e., from laminar to turbulent flow regime). The numerical approach takes into account the aspects of the fluid flow at higher Reynolds number values including circumferential velocity profiles at different cross-sections within the Kenics mixer, which were neglected in previous studies. It was observed that cross-sectional mixing in the turbulent flow regime takes place up to 30% of each element length at element-to-element transition; beyond that velocity profiles were uniform. The experiments were also carried out to measure the circumferential and axial velocity profiles and pressure drop in three different Kenics Mixers using air as fluid. The pressure drop per unit element ($\Delta P/\eta$) was found to be independent of the number of Kenics mixing elements used in the system. The total pressure drop across Kenics mixer obtained by CFD simulations were compared with the experimental pressure drop values and correlations available in the literature. The numerical results were found in good agreement with the experimental as well as the results reported in the literature. A new pressure drop correlation in the Kenics static mixer has been developed.

Keywords: Kenics static mixer; Motionless mixers; CFD; Circumferential and axial velocity profiles; Laminar flow; Turbulence flow; k–ω model; k–ε model

1. Introduction

Static mixer is a device consisting of a series of flow orientation elements inserted along the axis of pipe. Pressure drives the fluid through the device, providing the energy needed to accomplish mixing. Static mixers find applications in variety of industries, ranging from polymer processing, and biotechnology to water treatment. Thakur et al. [1] reported an extensive review on fluid flow and mixing of different types of static mixers. However, despite widespread use, fluid flow and mixing performance in theses device has not been rigorously characterized. The scarcity of information about flow and mixing in static mixers is partially available due to their often-complex construction, which makes direct, non-intrusive experimental investigations difficult. The analytical solutions for velocity fields are also impractical due to the complex geometry of static mixers. Numerical simulations were carried out to study the mixing performance of Kenics mixer [2–4]. However, in the above numerical studies the complex velocity fields were simplified by ignoring the flow developments at the transition between mixer elements in order to obtain an analytical solution for the axial, radial, and rotational flows.

Computational fluid dynamics (CFD) is an increasingly effective alternative to speed up equipment design and gain additional fundamental understanding of mixing process. Hobbs and co-workers [5–7] and Byrde and Sawley [8] numerically studied the helical static mixer for both the creeping flow and the laminar flow regimes (i.e., $10^{-5} < N_{Re} < 1000$). They reported that the flow transition at entrance and exit of each element strongly affect the velocity field up to ~12.5% of the element's length under creeping flow condition. Avalosse and Crochet [9] studied the flow behaviour of colored clay in the Kenics static mixer by finite element simulation and compared their simulation with the experimental results. Rauline et al. [10] used a commercial CFD package to model the creeping flow ($N_{Re} = 5 \times 10^{-4}$) in six different static mixer designs. Zalc et al. [11] studied the flow and mixing characteristics of the SMX mixer over a wide range of Reynolds numbers ($10^{-4} \leq N_{Re} \leq 10^{2}$). They reported

* Corresponding author. Tel.: +91 11 26591020; fax: +91 11 26591020.
E-mail address: nigamkdp@gmail.com (K.D.P. Nigam).

1385-8947/$ – see front matter © 2007 Elsevier B.V. All rights reserved.
doi:10.1016/j.cej.2007.07.101

Nomenclature

a	number of mixing elements
d	radial distance from wall (m)
D_t	diameter of tube
K	consistency coefficient in power law equation (N s^{n-2}/m^2)
L	length of the mixer (m)
n	power law index
N	number of layers generated
ΔP	pressure drop across Kenics mixer (Pa)
ΔP_0	pressure drop across empty pipe (Pa)
Re	$\rho D_t \bar{u}/\mu$ Reynolds number
$\bar{u}$	average velocity of fluid (m/s)
Z	pressure drop normalized to empty pipe ($\Delta P/\Delta P_0$)

Greek letters

η	number of mixing elements in the Kenics mixer
μ	viscosity of fluid (kg/m s)
ρ	density of fluid (kg/m^3)
ε	porosity

that the flow is independent of N_{Re} for $N_{Re} = 1$, while substantial deviations occur at increasingly higher Reynolds numbers where inertial forces are significant. Sazlai and Muzzio [12] reported that the only twist angle affects mixing performance at low flow rates ($N_{Re} \cong 1$), both the element aspect ratio and the twist angle are shown to be important at high flow rates ($N_{Re} \leq 1000$). All above-mentioned studies were limited to low values of Reynolds number.

Lang et al. [13] used a commercial CFD code (TASCflow) to predict the turbulent flow in a Sulzer SMV mixer that was used in a process stream for the denitrification of emissions from a power plant. However, to solve the problem given their available computer resources, they assumed that the static mixer was infinitely tall and wide by using periodic boundary conditions in the cross-stream directions. Jones et al. [14] have simulated turbulent flow in a static mixer using CFD for only one value of Reynolds number ($N_{Re} = 100{,}000$). They reported that the flow field within the mixer is characterized by the presence of pockets of reversed flow and the growth and interaction of strong longitudinal vortices.

Table 1
Geometry of Kenics mixing elements and fluid properties

Mixer	Kenics fluid		Air (NTP)
Diameter (m)	0.0254	Density (kg/m^3)	1.225
Length of element (m)	0.0381	Viscosity (kg/m s)	1.7894e-05
Blade thickness (m)	0.002		
Entrance and exit length (m)	0.01		
No. of elements	3, 9 and 25		

The objective of the present work is to characterize and investigate the effect of flow rate and number of elements on the complex hydrodynamics of turbulent flows and pressure drop predictions in Kenics static mixers using three-dimensional approach. The velocity fields and pressure drop reported in Kenics static mixer comprise of 3, 9 and 25 Kenics mixing elements over a wide range of Reynolds number ranging from 1 to 25,000 using commercial CFD software (FLUENT 6.2). The CFD simulations were also validated by comparing the velocity fields and pressure drop predictions with the experimental values and available correlations of pressure drop in a Kenics mixer. The experiments were carried out with air as a flowing fluid in Kenics mixer. New pressure drop correlations for a Kenics static mixer is also developed for the entire range of Reynolds number considered.

2. Geometry and fluid properties

The commercial static mixer chosen for the present study was a Kenics static mixer. Fig. 1a shows the geometry considered

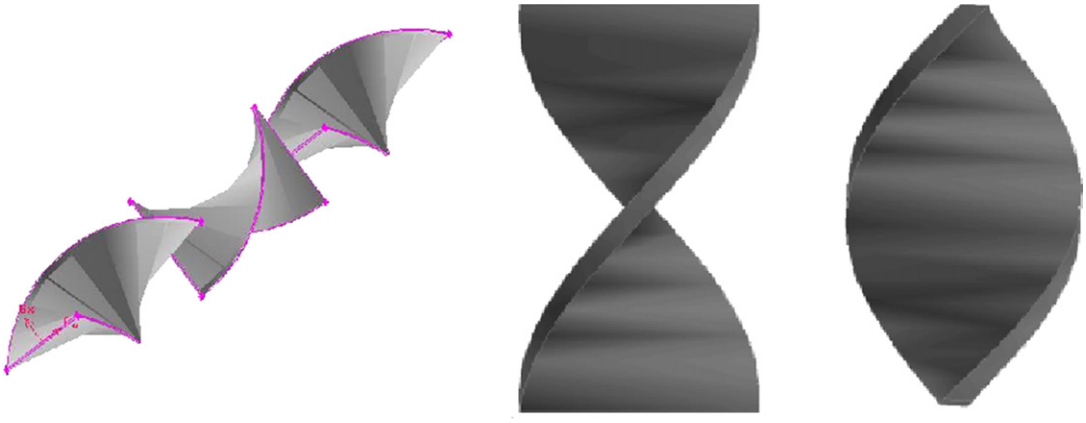

Fig. 1. Schematic diagram of 3 element Kenics Mixer.

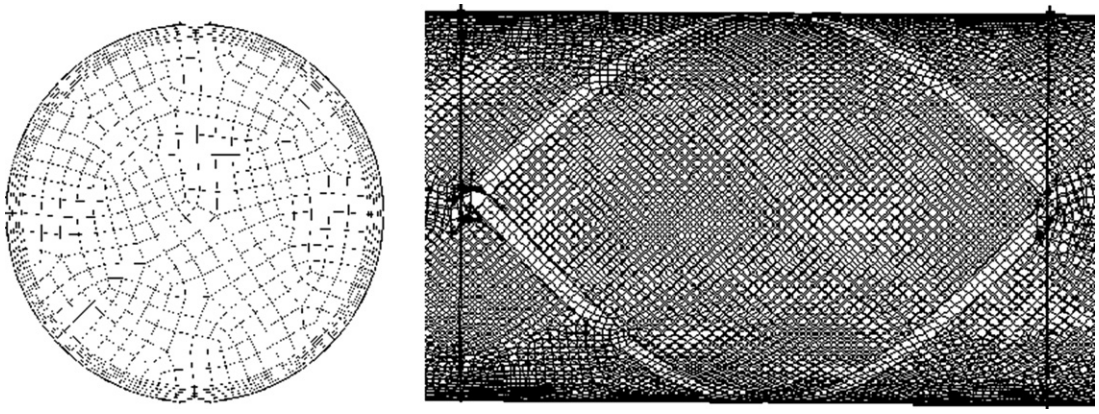

Fig. 2. Cross-sectional and axial grid topology of the Kenics static mixer.

for experimental and modelling of static mixers containing 3 standard Kenics inserts. A single insert is shown in Fig. 1b. The Kenics static mixer was comprised of a series of mixing elements, each consisting of a short helix, with having aspect ratio of 1.5 (i.e., $L/D = 1.5$) and twist angle 180°. These right handed and left handed elements were placed one after another. The leading edge of each element is at 90° to the trailing edge of the preceding element as shown in Fig. 1a. This will generate the alternating clockwise and counterclockwise rotation. The detailed dimensions along with the fluid properties are reported in Table 1.

3. Numerical computation

The flow during the simulations was assumed to be three dimensional, steady and incompressible. The simulations were performed using Fluent 6.2 (Fluent Inc., Lebanon, NH, USA). The geometries of the mixers were laid out using the grid generator Gambit 2.0 (Fluent Inc.), and unstructured tetrahedral meshes of the fluid volumes were constructed using TGrid (Fluent Inc.). The meshes were then exported to Fluent 6.2. The governing equations for continuity and momentum in the Kenics mixer were solved in the master Cartesian coordinate system with a control volume finite difference method (CVFDM).

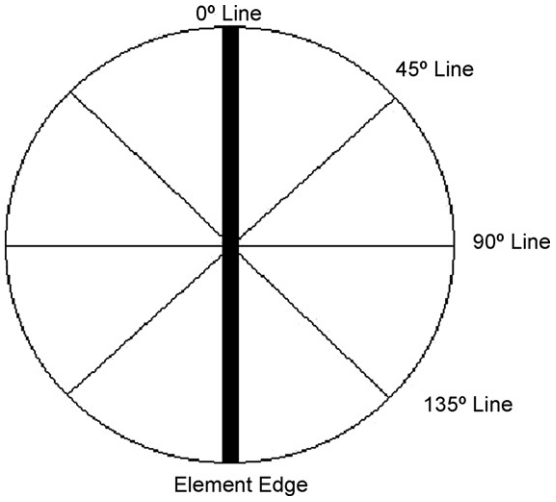

Fig. 3. Plane of measurement downstream of elements.

Fig. 2 shows three-dimensional unstructured mesh. The number of grids used in the mixer was from 469,451 to 4,930,240 depending upon the mixer configuration. The grid density test was performed to determine the appropriate grid distribution to assure accurate predictions of pressure drop values. The Kenics mixer geometry was meshed using different grid densities varying from 2 to 12 nodes per cm^3 per element, the number of control volumes being doubled until the pressure drop values

Table 2
Z values for various mixers in the laminar regime of flow

Types of mixer	*Z* values	Reference
Kenics	7	Pahl and Muschelknautz [17]
	$7.2 + Re/32$ for $Re < 50$	Wilkinson and Cliff [18]
	$4.86 + 0.65Re^{0.5}$ for $Re < 10^3$	Grace [19]
	$0.412Re^{0.5}$ for $Re < 10^2$	Morris and Mission [20]
	$5.4 + 0.028Re$ for $Re < 20$	Cybulski and Werner [21]
	$5.34 + 0.0211Re$ for $Re < 2300$	Sir and Lecjack [22]
	$2.03Re^{3/8}$ for $10 < Re < 1000$	Genetti [23]
IEAP PK	5.5–6.5	Cybulski and Werner [21]
IEAP PK	$9.2Re^{0.07}$ for $5.5 < Re < 127$	Dylag and Pyc [24]
Lightnin	9	Pahl and Muschelknautz [17]
	$7.4 + 0.7Re$	Cybulski and Werner [21]
N-Form	15–17	Pahl and Muschelknautz [17]
Komax	25	Pahl and Muschelknautz [17]
Hi-Torey	38	Pahl and Muschelknautz [17]
Sulzer SMX	10–100	Pahl and Muschelknautz [17]
Sulzer SMV	65–300	Pahl and Muschelknautz [17]
Ross ISG	250–300	Brunemann and John [25]

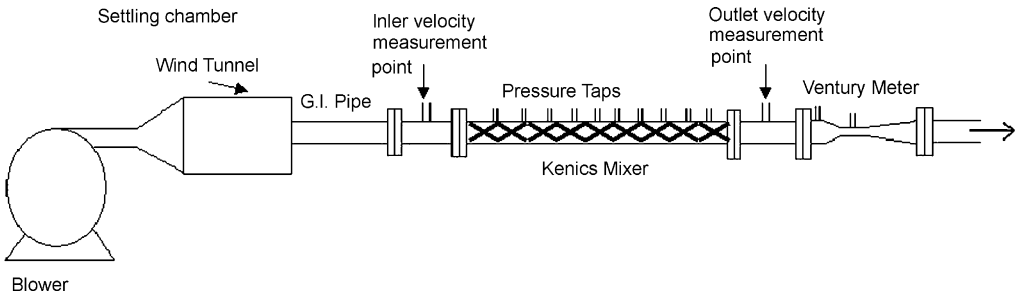

Fig. 4. Schematic layout of the experimental setup.

were obtained less than 1% for the two successive grid densities. The final grid density considered in the present work was 8 nodes/cm^3. The Mesh distribution was carried out at Reynolds number equals to 25,000, which is the maximum value of flow rate considered in the present work. The same node density per element was considered for the other mixer configurations. For calculating the turbulent flow in the static mixer the k–ω turbulence model was used because it has been validated extensively in complex, three dimensional shear flows and has better performance over k–ε model [15,16]. Simulations were also carried out using k–ε model with enhanced wall treatment to compare both the turbulence models under similar process conditions. The k–ε model with standard wall function requires that the cells near the wall should meet the y+ requirements. Therefore, a fine grid was considered near the wall.

To solve the velocity fields and pressure in the static mixer the second order discretization scheme was used for pressure equation. The coupling between the pressure and velocity was resoled using SIMPLEC scheme and the momentum calculations were carried out by second order upwind scheme.

The boundary condition used at the inlet was a fully developed velocity profile. A user-defined function (UDF) has been built to generate fully developed velocity profiles at the inlet of the static mixer. The uniform velocity profiles were also fed at the inlet of the Kenics static mixer and the velocity profiles at the outlet were measured. It was observed that there is no effect of inlet conditions on the outlet velocity profiles, which is also reported in the literature. All solid boundaries were stationary, with no-slip conditions applied. At the outlet the diffusion flux for all the variables in exit direction were set to be zero. Fluid properties

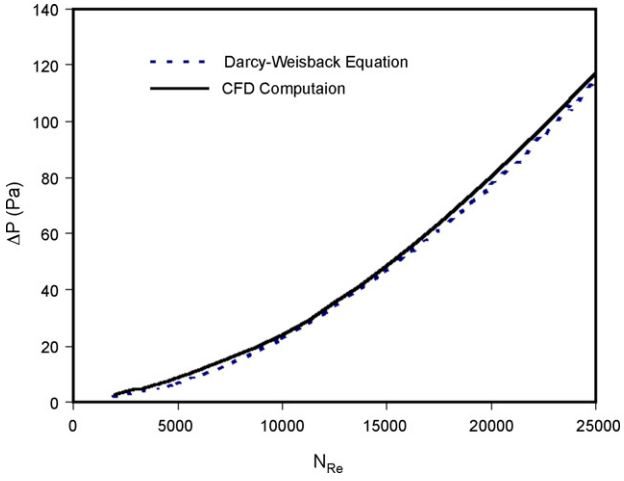

Fig. 5. Comparison of empty pipe pressure drop.

Table 3
Values of b and c in Eq. (3)

Mixer	Regime of flow	b	c	Reference
Sulzer SMV	$Re < 10$	5600	1	Pahl and Muschelknautz [27]
Sulzer SMX	$Re < 10$	3800	1	Pahl and Muschelknautz [27]
		2400	1	Cybulski and Werner [21]
Sulzer SMXL	$Re < 10$	590	1	Pahl and Muschelknautz [27]
		500	1	Cybulski and Werner [21]
Kenics	$Re < 10$	450	1	Pahl and Muschelknautz [27]
	$Re < 20$	295	1	Cybulski and Werner [21]
	$Re < 20$	12.6	0.5	Morris and Mission [21]
	$1200 < Re < 6700$	10.9	0.4	Cybulski and Werner [22]
Ross ISG	$Re < 10$	12000	1	Pahl and Muschelknautz [27]
Ross LPD	$1200 < Re < 6700$	25	0.44	Cybulski and Werner [21]
Hi-Toray	$Re < 10$	2100	1	Pahl and Muschelknautz [27]
Komax	$Re < 500$	1640	1	Cybulski and Werner [21]
	$1200 < Re < 6700$	9.96	0.0022	Cybulski and Werner [21]
CBMiM	$1200 < Re < 6700$	27.6	0.53	Cybulski and Werner [21]
IchP	$1200 < Re < 6700$	7.3	0.37	Cybulski and Werner [21]

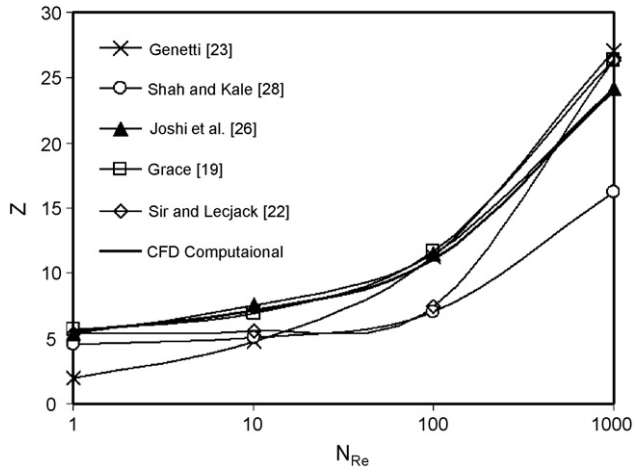

Fig. 6. Predicted relative pressure drop as a function of Reynolds number.

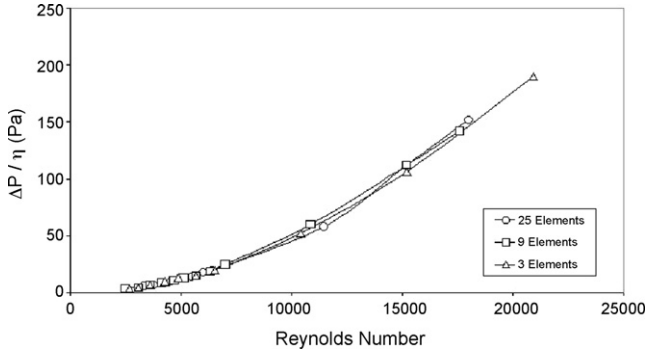

Fig. 7. Pressure drop per unit element vs. Reynolds number.

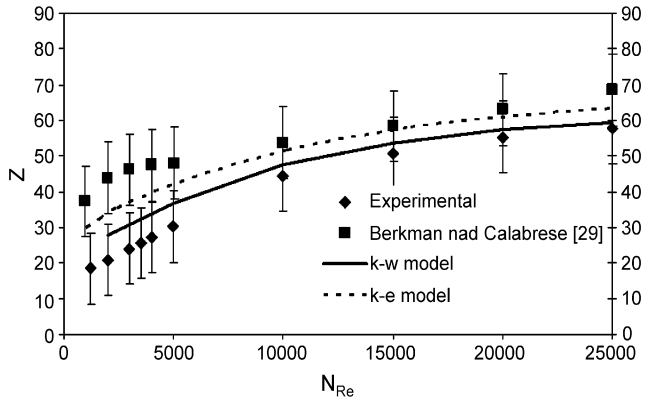

Fig. 9. Predicted relative pressure drop vs. Reynolds number.

used in the simulations are given in Table 1. The numerical computation was considered converged when the residual summed over all the computational nodes at nth iteration R^n_ϕ, satisfies the criterion: $R^n_\phi / R^m_\phi \leq 10^{-5}$, where R^m_ϕ denotes the maximum residual value of ϕ variable after m iterations, ϕ applied for p and u_i.

The outlet velocity profile and pressure drop per element ($\Delta P/\eta$) were obtained via iteration on a Sun Blade 2000 workstation. The outlet pressure was measured on a plane, which was at 7.5 cm distance from trailing edge of the last element. This distance was chosen so as to allow the wake of the blade to decay and we would get the precise value of pressure at the outlet. The circumferential and axial velocities were also measured on the same plane on different lines as shown in Fig. 3. The 0° line corresponds to the plane, which is inline with the edge of the last element. The other lines were identified as 45°, 90° and

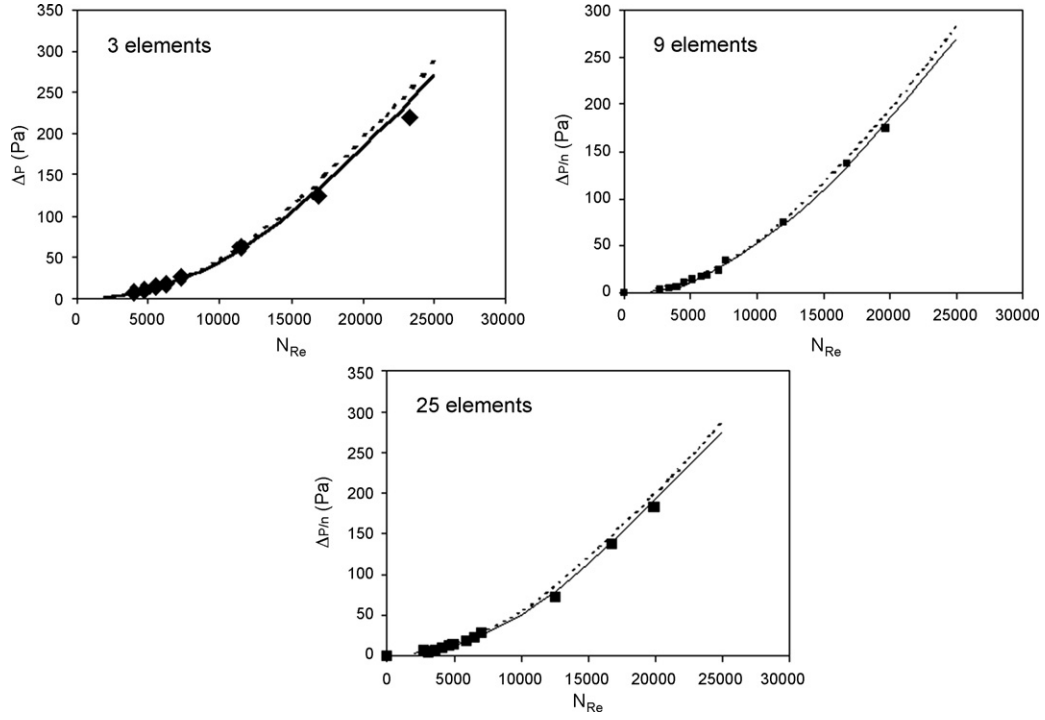

Fig. 8. Pressure drop per unit element (DP/h) vs. Reynolds number (♦ experimental; ▬ *k–(* (computational) and - - - *k–(* (computational).

135° with 0° line. In addition to the Kenics mixers elements, an entrance and an exit sections for the mixer were also simulated. The entrance and exit sections were modelled as open tubes with the same diameter as the mixer elements (2.54 cm) and a length of 4-tube diameter (10.16 cm).

4. Experimental details

A systematic experimental diagram of the setup is shown in Fig. 4. It consists of blower for supplying air, settling chamber with honeycomb and screen. The air from the blower passes

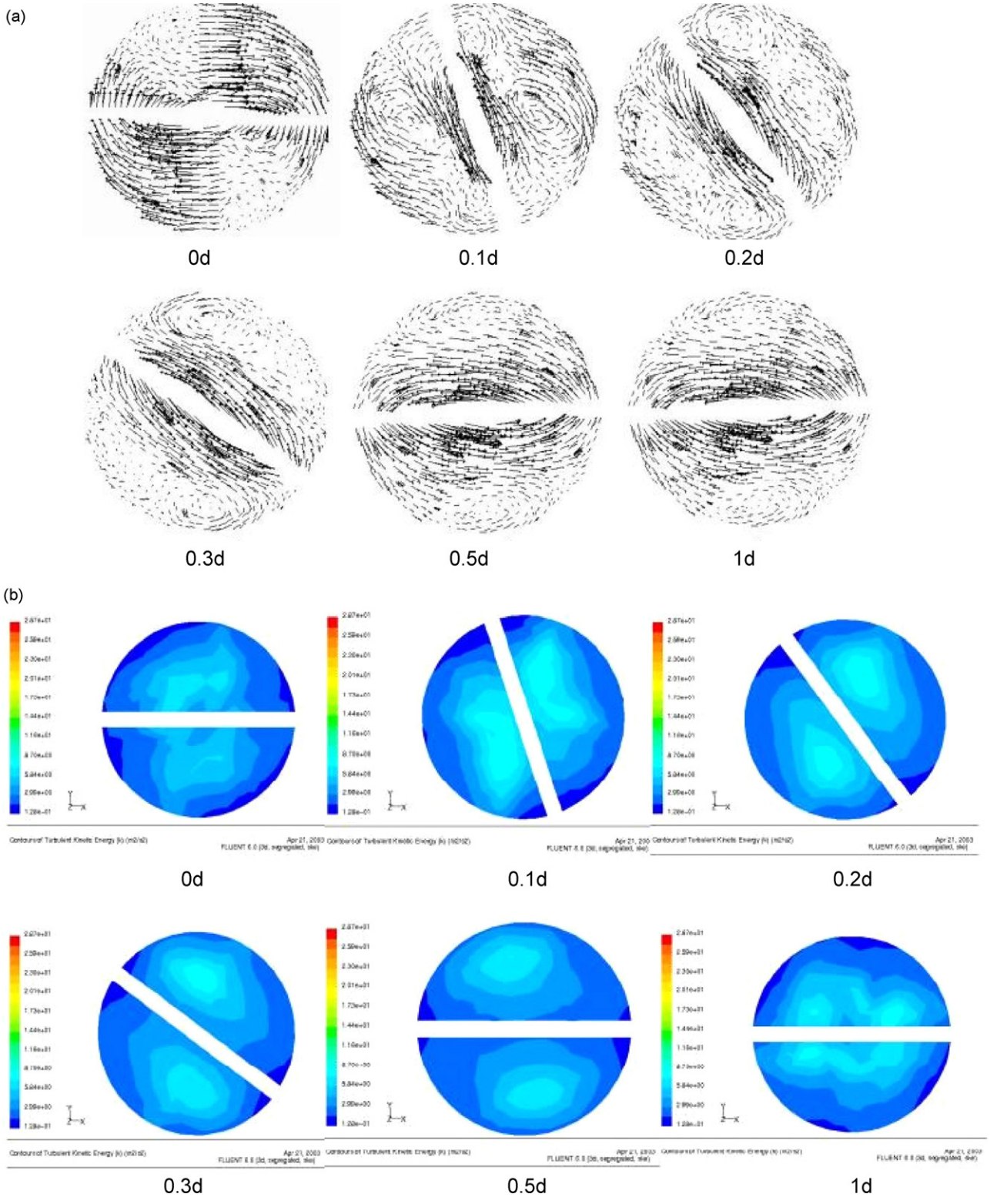

Fig. 10. (a) Circumferential velocity (m/s) and (b) turbulence kinetic energy (m^2/s^2) at various cross-sections at third element of 25 elements Kenics mixer.

through the settling chamber into the G.I. pipe of diameter 2.54 cm and length of 127 cm through a well guided bell mouth entry provided in settling chamber. The G.I. pipe was connected to a Perspex tube, which contains a series of Kenics mixing elements. A number of pressure outlets were provided on this pipe to enable the measurement of pressure drop along the length of Kenics elements. The Kenics mixing elements required for the present study were fabricated at IIT Delhi by twisting a stainless steel sheet of 0.2 cm thickness. An upstream and downstream length of 10 cm was provided. A venturi meter was connected downstream of the pipe for measurement of the flow rate. The air flow rate was varied by increasing the rpm of the impeller in the blower. A three-hole probe of diameter 0.3 cm was used to measure the velocity profile (axial, radial and circumferential) using Betz micro-manometer (least count 0.1 mm of water).

5. Results and discussion

5.1. Pressure drop

There are number of correlations proposed by various authors for calculating the pressure drop under laminar flow conditions in the Kenics mixer. The pressure drop in a static mixer has been

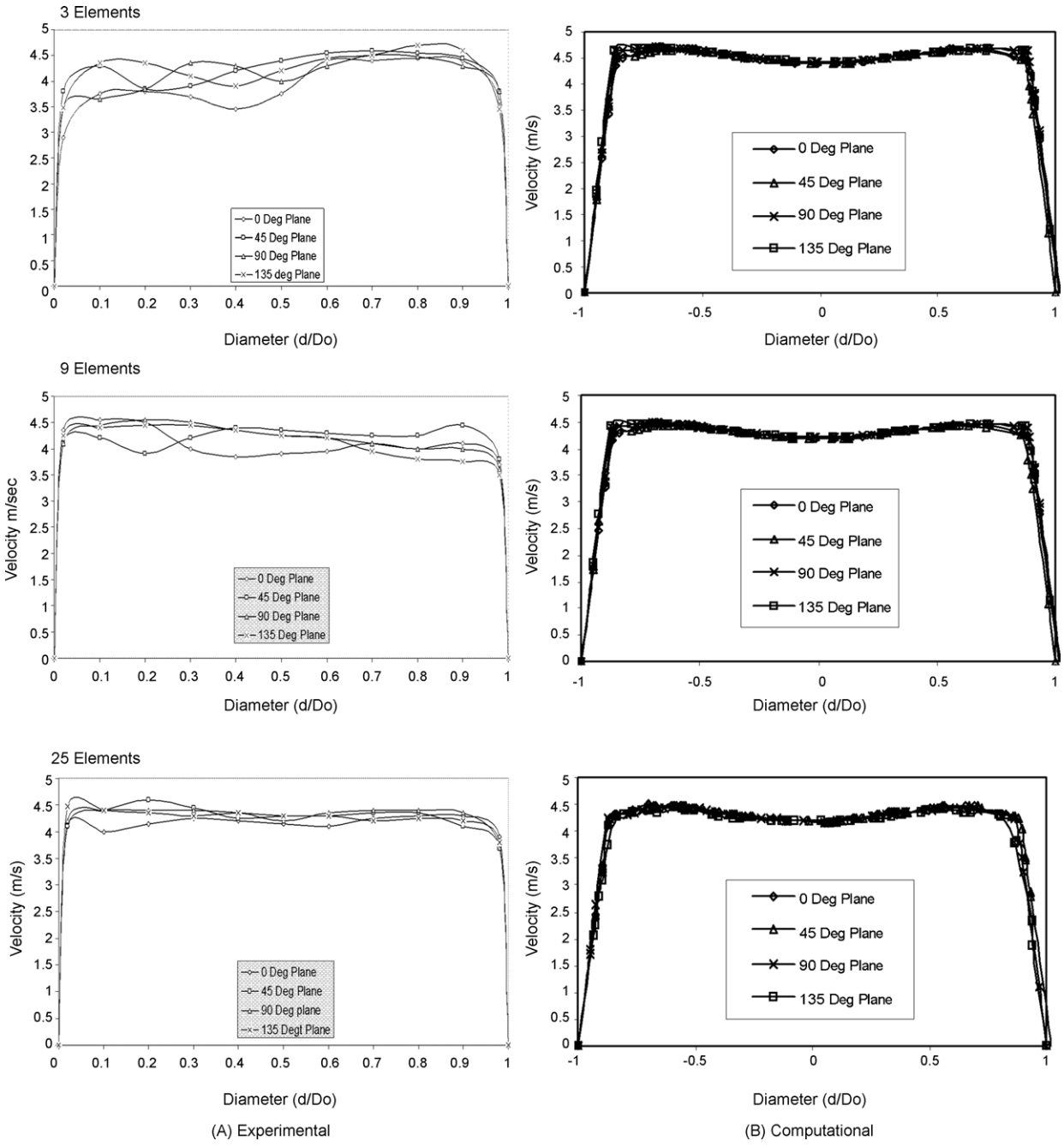

Fig. 11. Axial velocity distribution at downstream of elements at $Re = 6000$.

reported by two ways in the literature:

(1) The ratio of the pressure drop across the mixer to that across an open pipe of the same diameter and length, i.e.,

$$Z = \frac{\Delta P}{\Delta P_0} \tag{1}$$

Table 2 summarizes the equations reported in literature to calculate the value of Z.

(2) A resistance coefficient in the Darcy-Weisbach equation

$$\Delta P = \lambda \frac{L}{D} \frac{\rho \bar{u}^2}{2} \tag{2}$$

which is correlated as

$$\lambda = \frac{b}{Re^c} \tag{3}$$

for large values of *Re*, the resistance coefficient approaches a constant value. Table 3 lists the values of coefficients *b* and *c* in Eq. (3). Joshi et al. [26] reported the following empirical

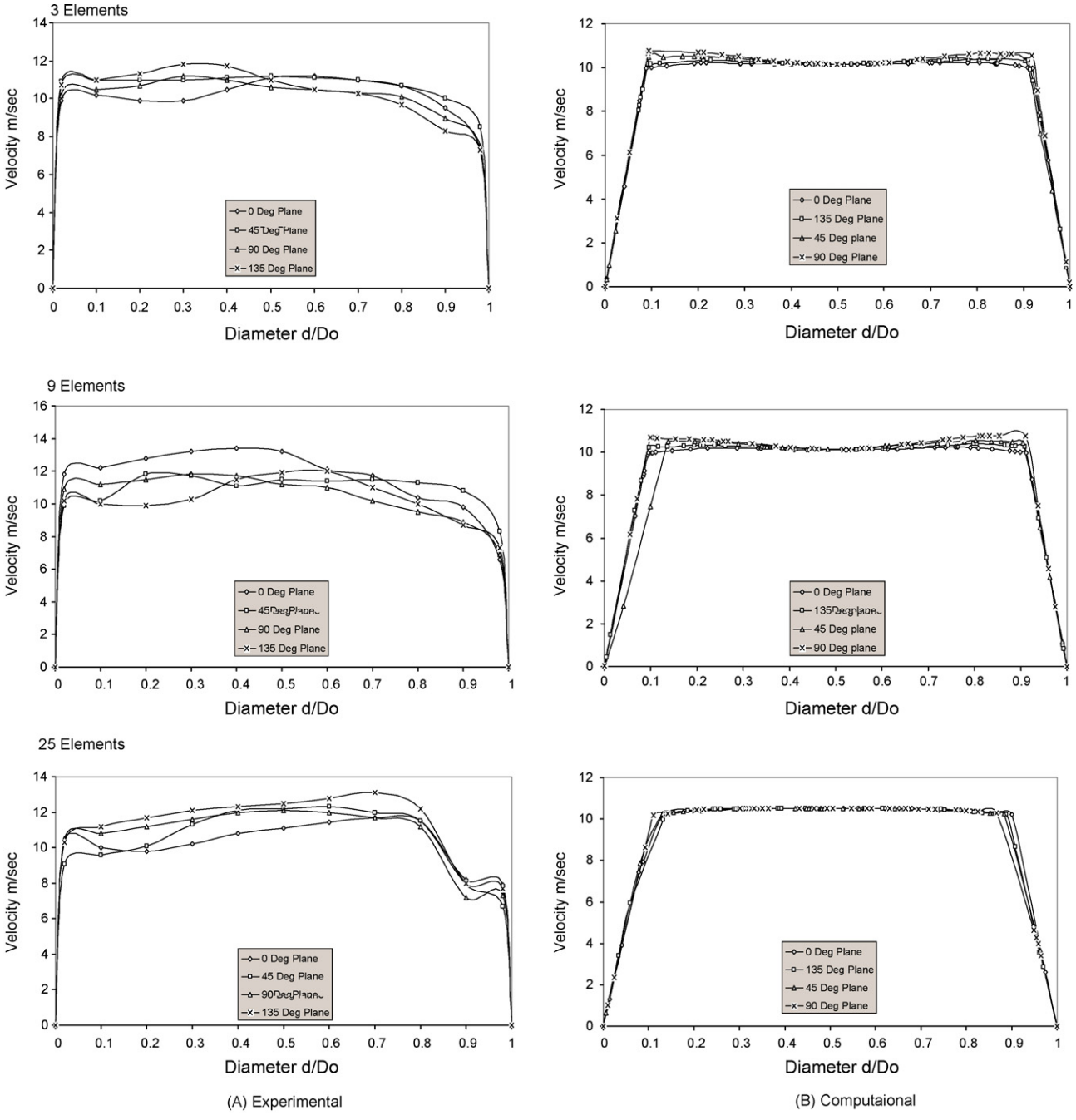

Fig. 12. Axial velocity distribution at downstream of elements at *Re* = 18000.

equation to calculate the value of ΔP and ΔP_0.

$$\frac{\Delta P}{\frac{1}{2}\rho\bar{u}}\frac{D_t}{L} = 30.3\, Re_h^{-0.488}\mathrm{Ra}^{-1.04} \quad (4)$$

$$\Delta P_0 = \frac{32\,\mu\bar{u}L}{D_t^2} \quad (5)$$

For the higher Reynolds numbers, less attention has been made for the pressure drop correlations in the literature. Pahl and Muchelknautz [17,27] and Cybulski and Werner [21] reported the correlations for the friction factor for two different range of Reynolds number s, $1200 < Re < 7000$ and $7000 < Re < 30{,}000$, respectively. The correlation used for turbulent flow was similar to the Eq. (3). Fig. 5 shows the comparison between the pressure drop in an empty tube obtained by CFD and the available correlation of Darcy-Weisback equation. The present study shows the accuracy of CFD predictions of pressure drop with Darcy-Weisback equation results within ±2%.

Fig. 6 represents the comparison of the Z values obtained by CFD with several correlations available in literature in laminar region. The Reynolds number was varied from 1 to 1000. It can be seen from the Fig. 6 that there is a wide variation among the different correlations reported in the literature. Fig. 6 shows that the CFD predictions for Z values were in good agreement

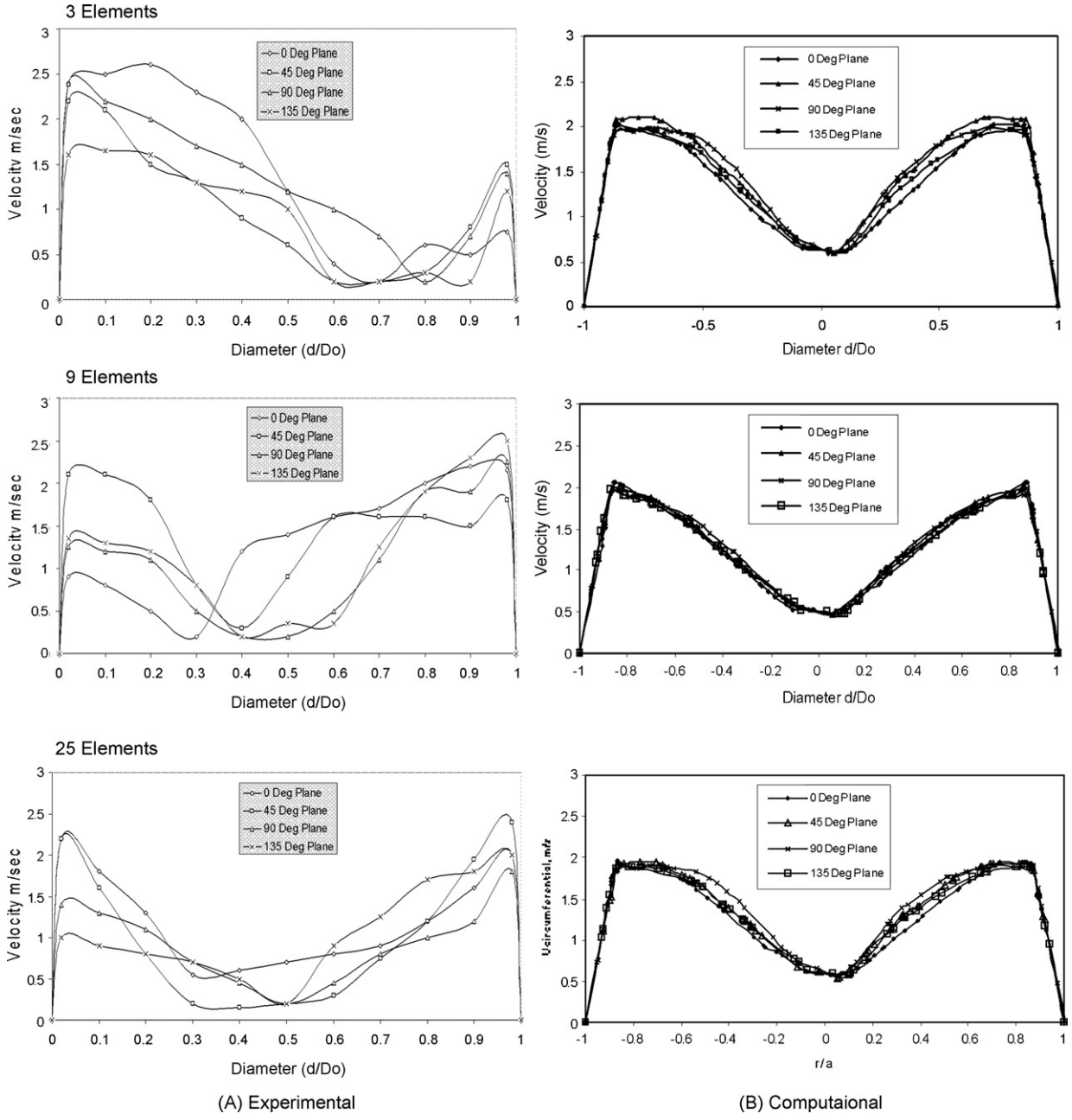

Fig. 13. Circumferential velocity profile at downstream of elements at $Re = 6000$.

(±4%) with results reported by Joshi et al. [26] over the entire range of Reynolds number ($1 < N_{Re} < 1000$).

The experimental variation of $\Delta P/\eta$ with Reynolds number in static mixer is reported in Fig. 7 with 3, 9 and 25 Kenics mixing elements. It can be observed from Fig. 7 that the pressure drop per unit element ($\Delta P/\eta$) does not change significantly with increase in number of elements. The experimental measurement of total pressure drop across static mixer was empirically correlated by the following equations.

$$Z = \frac{\Delta P}{\Delta P_0} = 0.0031 N_{Re} + 14.69 \quad \text{for } 1000 < N_{Re} < 10,000 \tag{6}$$

$$Z = \frac{\Delta P}{\Delta P_0} = 0.023 N_{Re} - 4 \times 10^{-8} N_{Re}^2 + 25.36$$

$$\text{for } 10,000 < N_{Re} < 25,000 \tag{7}$$

The $\Delta P/\eta$ was also computed for Reynolds number ranging from 1000 to 25,000 and results were compared with experimental data. The simulations were conducted with both k–ω as well as k–ε models. The computational results of k–ε and k–ω models for $\Delta P/\eta$ are reported in Fig. 8 along with experimental results. It can be seen from the Fig. 8 that the k–ω model predictions are in very close agreement with the experimental data as compared to the k–ε model. The maximum deviations of k–ω model from experimental data were found to be less than 5% for all the three Kenics mixer units.

A literature search for pressure drop in turbulent region in Kenics static mixer shows only one experimental study by Berkman and Calabrese [29]. The predictions from Eqs. (6) and (7) along with the CFD predictions using k–ω and k–ε models are reported in Fig. 9. Fig. 9 also shows the experimental data of Berkman and Calabrese [29]. It can be seen from the Fig. 9 that

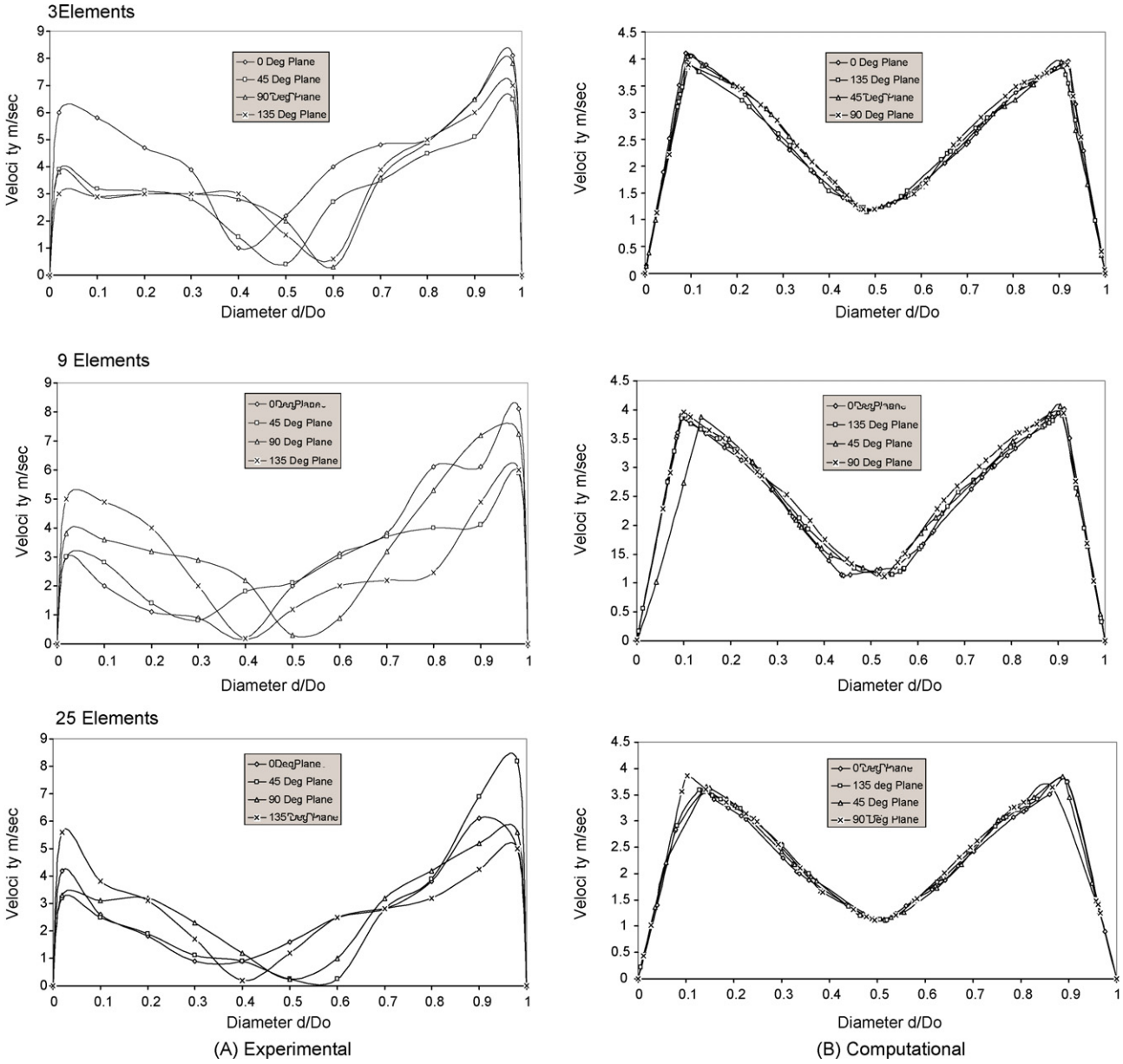

Fig. 14. Circumferential velocity profile at downstream of elements at $Re = 18,000$.

CFD results lies between experimental results of Berkman and Calabrese [29] and present experimental data. It can also be seen from the Fig. 9 that the results obtained using k–ε turbulence model are in well agreement with the Berkman and Calabrese [29] and present experimental predictions are in good agreement with the k–ω turbulence model predictions.

5.2. Transition length

Fig. 10a shows the circumferential velocity at the various cross-sections of the third element of a mixer having 25 Kenics mixing elements. It was observed that velocity profiles were affected greatly in the area of element-to-element transition and this effect can be seen up to 30% of the element length. In later 70% of the element length, velocity profiles were uniform and there is not much cross-sectional mixing in the fluid. The turbulent kinetic energy (TKE) expresses the dynamics of the kinetic energy due to the velocity fluctuations of a turbulent flow, which is also presented in Fig. 10. It can be seen from the Fig. 10b, the turbulent kinetic energy at the various cross-section of the third element of a mixer having 25 Kenics mixing elements shows the same phenomenon as shown in the Fig. 10a.

5.3. Velocity profiles

The axial velocity profiles were measured at a distance of 7.5 cm from the trailing edge of the last element to lean out the effect of the wake formed by the element. The comparison of the axial velocity profiles obtained at 6000 and 18,000 Reynolds number by CFD simulation and experiments are reported in the Figs. 11 and 12, respectively. The difference between experimental results and CFD predictions was observed, which may be due to the error in experimental measurements. Figs. 11 and 12 show that the axial velocity distribution are relatively similar in order and magnitude from experimental and CFD predictions. For higher number of elements ($n = 25$) the flow patterns from CFD predictions are relatively similar with the experimental results for value of Reynolds number equal to 6000. However at higher Reynolds number ($Re = 18000$) the axial velocity distribution is fairly agrees with the experimental results in both order and magnitude. It can also be seen that the axial and circumferential velocity profiles are more flat in 25 Kenics mixing elements system than 3 and 9 elements systems. Similarly, the circumferential velocity distribution shows a forced vortex nature at the centre of the tube and nearly free vortex near the wall as shown in the Figs. 13 and 14, respectively. It can be seen from Fig. 14 that the circumferential velocity profiles from CFD simulations are in relatively good agreement with the experimental predictions at higher value of Reynolds number ($Re = 18000$).

6. Conclusion

In the present study, three-dimensional CFD simulations were carried out for three different Kenics static mixer over a wide range of Reynolds number ($1 \leq N_{Re} \leq 25{,}000$). Experiments were also carried out on physical system using air as fluid. A new correlation was developed (Eqs. (6) and (7)) to calculate the total pressure drop in Kenics static mixer. From the CFD simulation and experiments, it was observed that the pressure drop per unit element in Kenics static mixer increases with increase in Reynolds number. The rise in pressure drop across Kenics static mixer was steep at higher Reynolds number. The pressure drop obtained from CFD simulation was compared to several experimental correlations available for laminar flow in the literature and found in good agreement with Joshi et. al. [26] over the entire range of Reynolds number ($1 \leq N_{Re} \leq 1000$). For the higher values of Reynolds number the CFD predictions using k–ε and k–ω turbulence models were lies between the predictions of Berkman and Colabrosse [29] and the present experimental predictions. Analysis of the velocity field within the Kenics mixer indicates that flow was affected in the region of element-to-element transition up to 30% of the element length and flow was well developed in the other region of element. Comparison of the circumferential velocity profiles indicates that there was formation of forced vortex in central part of the tube and free vortex near the wall. The CFD predictions were in relatively good agreement with the experimental results for axial and circumferential velocity fields for higher Reynolds number

Acknowledgment

The authors gratefully acknowledge the Ministry of Chemical and Fertilizers, GOI, India for funding the project.

References

[1] R.K. Thakur, Ch. Vial, K.D.P. Nigam, E.B. Nauman, G. Djelveh, Trans IchemE 18 (Part A) (2003) 787–823.
[2] J. Arimond, L. Earwin, J. Eng. Ind. Trans. ASME 107 (1985) 70–76.
[3] K. Dackson, E.B. Nauman, Chem. Eng. Commun. 54 (1987) 381–394.
[4] F.H. Ling, X. Zhang, Chem. Eng. Commun. 136 (1995) 119–141.
[5] D.M. Hobbs, F.J. Muzzio, Chem. Eng. J. 70 (1998) 93–104.
[6] D.M. Hobbs, Characterization of a Kenics static mixer under laminar flow conditions, PhD thesis, Rutgers, State University of New Jersey, New Brunswick, N.J., 1998.
[7] D.M. Hobbs, P.D. Swanson, F.J. Muzzio, Chem. Eng. Sci. 53 (1998) 1565–1584.
[8] O. Byrde, M.L. Sawley, Chem. Eng. J. 72 (1999) 163–169.
[9] Th. Avalosse, M.J. Crochet, AIChE J. 43 (1997) 3.
[10] D. Rauline, P.A. Tanguy, J.-M.L. Bleĭvec, J. Bousquet, Can. J. Chem. Eng. 76 (1998) 527–535.
[11] J.M. Zalc, E.S. Sazlai, F.J. Muzzio, S. Jaffer, AIChE J. 48 (2002) 427.
[12] E.S. Sazlai, F.J. Muzzio, AIChE J. 48 (2002) 427.
[13] E. Lang, P. Drtina, F. Streiff, M. Fleischli, Int. J. Heat Mass Trans. 38 (1995) 2239–2250.
[14] S.C. Jones, F. Sotriopoulos, A. Amrithrajah, J. Environ. Eng. 431 (2002).
[15] F.-B. Lin, F. Sotiropoulos, J. Fluids Eng. 119 (1997) 314–324.
[16] F. Sotiropoulos, Y. Ventikos, AIAA J. 36 (1998) 1256–1262.
[17] M.H. Pahl, E. Muschelknautz, Chem. Eng. Technol. 52 (1980) 285–291.
[18] W.L. Wilkinson, M.J. Cliff, Paper presented at European Conference on Mixing, Cambridge, England, 1977.
[19] C.D. Grace, Chem. Proc. Eng. 52 (1971) 57–59.
[20] W.D. Morris, P. Misson, Ind. Eng. Chem. Process. Des. Dev. 13 (1974) 338–342.
[21] A. Cybulski, K. Werner, Intern. Chem. Eng. 26 (1986) 171–180.
[22] J. Sir, Z. Lecjack, Chem. Eng. Commun. 16 (1982) 325–334.
[23] W.E. Genetti, Chem. Eng. Commun. 14 (1980) 47–57.

[24] M. Dylag, M. Pyc, Inz. Ap. Chem. 19 (1980) 9–12.
[25] H. Brunemann, G. John, Chem. Eng. Technol. 51 (1971) 347–364.
[26] P. Joshi, K.D.P. Nigam, E.B. Nauman, Chem. Eng. J. 59 (1995) 265–271.
[27] M.H. Pahl, E. Muschelknautz, Chem. Eng. Technol. 51 (1979) 347–364.
[28] N.F. Shah, D.D. Kale, Chem. Eng. Sci. 46 (1991) 2159–2161.
[29] P.D. Berkman, R.V. Calabrese, AIChE J. 34 (1988) 602–609.